Journal of Constructional Steel Research 208 (2023) 108036

Contents lists available at ScienceDirect

Journal of Constructional Steel Research

journal homepage: www.elsevier.com/locate/jcsr

Experimental analysis of a full-scale steel frame with replaceable dissipative connections

Roberto Andreotti, Giulia Giuliani, Nicola Tondini *

Department of Civil, Environmental and Mechanical Engineering, University of Trento, Via Mesiano 77, 38123 Trento, Italy

ARTICLE INFO

Keywords:
Hybrid tests
Pseudodynamics
Steel braced frame
Seismic resilience
Replaceable connection
Hysteretic dissipation
Nonlinear calibration

ABSTRACT

This work presents the experimental campaign performed on a full-scale 6-storey steel concentrically braced frame equipped with the so-called Dissipative Replaceable Braced Connection (DRBrC) made with plates of mild steel and high-strength steel. Such component, constituting the brace-column joint, is capable of dissipating large amounts of energy through wide hysteretic loops, while providing the possibility of being easily replaced after the building undergoes medium-high intensity earthquakes. To reduce the costs and, at the same time to obtain a representative response of the full frame, hybrid simulation tests were employed, in which only the ground floor was physically built in the laboratory. In contrast, the remainder of the structure was numerically simulated. The innovative frame was subjected to three different natural ground motions at the Damage Limitation (DL), Significant Damage (SD) and Near Collapse (NC) limit states, respectively. The outcomes highlighted the high potential of the DRBrC component in dissipating large amounts of energy and, at the same time, in protecting the remaining parts of the structure, by exhibiting very small residual displacements that enhance self-centring and repairability capabilities. Moreover, the numerical models were calibrated by including the non-negligible effect introduced by the bolt-hole clearances. All results are thoroughly described in the manuscript.

1. Introduction

1.1. Background and motivation

Earthquakes are destructive and unpredictable events that may have catastrophic consequences for people and the built environment. Although the current standards allow for effective seismic design against life losses by applying the capacity design philosophy [1], large residual structural damage may determine enormous social and economic issues. Therefore, the way of dealing with the design and maintenance of civil structures is of primary importance, as discussed by McConnell et al. [2]. Therefore allowing for irreversible structural damage due to earthquakes cannot be considered an acceptable strategy for structural design nowadays, which should account for both short-term and long-term costs. Consequently, a low-damage strategy has raised a lot of attention in the engineering research community, among which the development of different devices for energy dissipation has taken place. In particular, partial strength joints in steel structures constitute a valid solution since the damage is localized in few components that could, in principle, be replaced after a strong seismic event [3–7]. As a matter of fact, partial strength joints have been demonstrated to be a considerable source of energy dissipation, which can further be increased by partial interaction between the steel beam and the concrete slab [8]. Moreover, friction connections allow the dissipation of large amounts of energy without experiencing high damage [9–11]. Slit dampers that were experimentally tested both for Eccentrically Braced Frames (EBF) [12] and Moment Resisting Frames (MRF) [13] demonstrated wide and compact hysteretic behaviour both in force–displacement and moment-rotation diagrams. Added damping and stiffness (ADAS and TADAS) dampers [14] showed suitable hysteretic behaviour under natural ground acceleration records, keeping the main structure undamaged. Moreover, new types of materials, different from classical carbon steel, were demonstrated to be suitable for hysteretic energy dissipation. For instance, stainless steel (SS) strain hardening properties could efficiently increase strength in buckling restrained braces (BRB) [15] and prevent local buckling in MRF and CBF structures [16]. Copper revealed to possess mechanical characteristics, such as high ductility, low-yield strength and high resistance to corrosion, that demonstrated to be suitable for practical applications, e.g. ADAS dampers [17].

Concentrically Braced Frame (CBF) solution is a popular choice of lateral-force resisting system that relies on the energy dissipated by the diagonals in tension because it avoids the design of complex and costly

* Corresponding author.
E-mail address: nicola.tondini@unitn.it (N. Tondini).

https://doi.org/10.1016/j.jcsr.2023.108036
Received 6 March 2023; Received in revised form 5 May 2023; Accepted 24 May 2023

moment connections, which instead are a typical feature of MRFs. However, despite the effectiveness of such a lateral-load resisting system to withstand seismic actions, two concerns arise: (i) poor dissipation in compression is exhibited because of buckling phenomena [18–20]; (ii) the damage subjected by the braces may hinder the post-earthquake functionality of the structure and consequently may entail occupant relocation and business downtime. Moreover, a large pinching effect is observable in the deformation reversal. For instance, using BRB is a suitable option to improve hysteretic performance, particularly in compression. However, the BRB behaviour is characterized by low post-yielding stiffness, which may lead to large residual inter-storey drifts. In addition, BRBs are sensitive to low-cycle fatigue fracture due to the limited cumulative ductility capacity [21–23]. In this context, several European projects were devoted to conceiving and testing innovative connections for steel structures designed as dissipative seismic fuses that are easy to replace after damage due to strong seismic action. They were collected in the dissemination project INNOSEIS [24]. In particular, an extensive experimental campaign analysed the behaviour of dissipative braced pinned connections in the INERD project [25] to be used in CBFs. Furthermore, another two components were studied, namely FUSEIS type 1 and 2, which are (i) a system of two stocky steel columns with several dissipative steel beams with reduced end cross sections (FUSEIS type 1) and (ii) an innovative dissipative replaceable connection for composite MRF (FUSEIS type 2) [26,27]. The results of the experimental campaign demonstrated an excellent energy dissipation capability due to stable hysteretic behaviour. Such novel solutions were tested on the single dissipative component, and their performance on large-scale tests was rarely investigated due to budget and equipment constraints. In this context, the hybrid simulation (HS) technique is an efficient tool that allows the reproduction of the seismic response of a large-scale structure by subdividing the testing domain into a physical subdomain (PS), which is built in the laboratory, and a numerical subdomain (NS), created in a computational environment running in parallel to the physical test. Thus, it is straightforward to employ HS also for testing dissipative connections at the level of the structural system based on realistic loading histories [7,28–32].

1.2. Research scope

It becomes clear that minimizing loss of structural functionality, yet guaranteeing large hysteretic dissipation capabilities to structures, are goals of primary importance to be simultaneously achieved in seismic design. Furthermore, there is a need to evaluate the effectiveness of innovative dissipative components by means of full-scale tests. On these premises, the European Research Fund for Coal and Steel (RFCS) pilot project DISSIPABLE [33] was funded with the aim to experimentally test large-scale innovative structures equipped with seismic fuses by means of shaking table tests and HS tests to demonstrate their favourable dissipative behaviour as well as their ease of replacement. The dissipative components called Dissipative Replaceable Braced Connections (DRBrC), Dissipative Replaceable Link Frame (DRLF) and Dissipative Replaceable Beam Splices (DRBeS) [7], which were respectively named after the previous projects INERD, FUSEIS type 1 and FUSEIS type 2, were tested. In particular, in this work, two CBFs representative of a six-storey building prototype and equipped with the seismic fuse originally developed in the INERD project [25], i.e. DRBrC, and improved within DISSIPABLE, were tested according to HS at the Material and Structures Testing Laboratory (MSTL) of the University of Trento (UNITN). The two frames differed by the steel grade employed to realize specific parts of the DRBrC component, namely S355, mild steel, and S460, high strength steel (HSS). Some of the results obtained in the experimental campaign were briefly reported in Mattei et al. [34], where comparisons with different numerical models were discussed. The main advancements provided in this work with respect to [34] are the following: (i) extensive presentation of the experimental results of the HS performed at UNITN; (ii) description of the technical insights about the HS technique employed in the experimental tests; (iii) presentation of both the nonlinear finite element calibration of the DRBrC components and implementation of such nonlinear elements in the numerical substructure (NS); (iv) comprehensive description of the experimental outcomes, that includes discussion on the dissipative behaviour of the DRBrC components, the elastic behaviour of the irreplaceable parts, the replaceability of the DRBrC components along with the self-centring capabilities. Furthermore, the main innovative contributions of this article are: (i) to investigate, through full-scale HS tests, the ability of the DRBrC components to dissipate large amounts of energy by protecting the non-dissipative members; (ii) to assess the ease of replacement of the DRBrC components in the context of enhanced structural seismic resilience and the Performance-Based Earthquake Engineering (PBEE) approach.

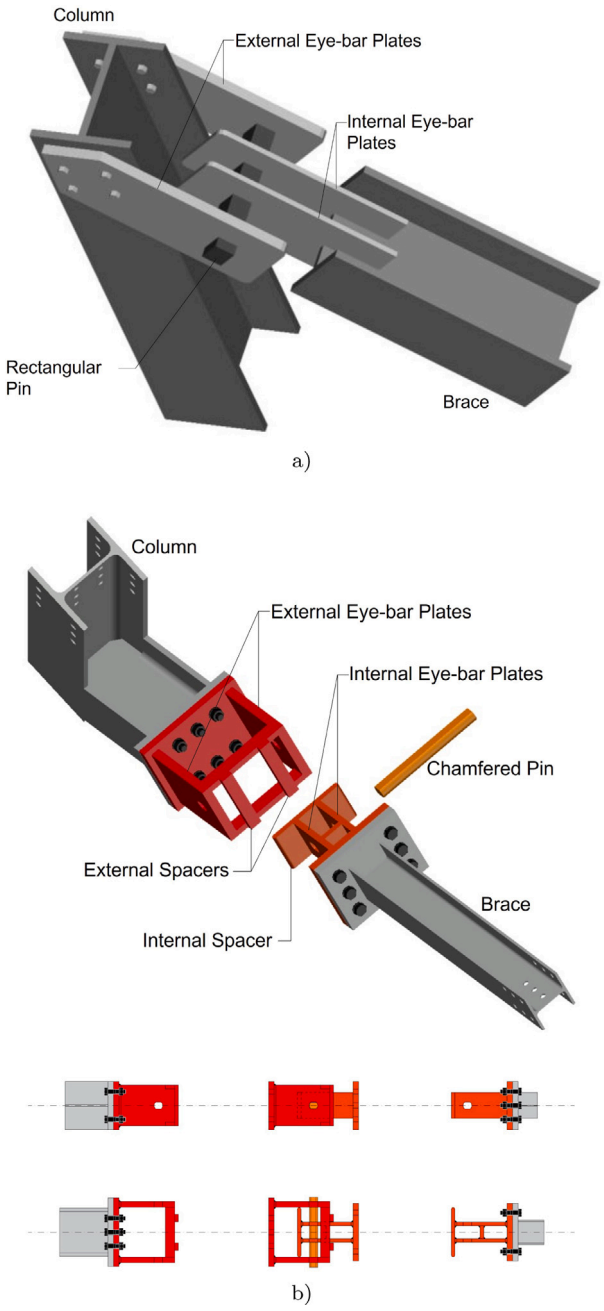

Fig. 1. Evolution of the dissipative component: (a) brace connection proposed in the INERD project [24]; (b) DRBrC proposed in the DISSIPABLE project.

2. Description of the Dissipative Replaceable Brace Connection (DRBrC)

The DRBrC is a dissipative component employed in a CBF and positioned at the ends of both bracing diagonals, that are designed to avoid buckling in compression and yielding in tension. Its main conception is shown in Fig. 1, both in its original (a) and improved (b) configurations. The connection, depicted in Fig. 1a, was first developed in the INERD project [25]: it consists of a pin, supported by two internal eyebar plates and two external ones, positioned at such a distance so that the pin is the dissipative component that behaves both in bending and shear. A large experimental campaign was conducted to deeply analyse the cyclic behaviour of the component, see Vayas et al. [35]. As a main outcome, despite an evident pinching owing to deformation reversal, a favourable dissipation capability due to a stable hysteretic behaviour of the connection was highlighted. The pinching effect was due to the clearance between the hole and the eyebar plates, as well as the ovalization of the hole and the out-of-plane flexural behaviour of the supporting eyebar plates. However, due to the pin large inelastic deformations, it was very difficult to be replaced [24]. For this reason, in the DISSIPABLE project, an improved solution to facilitate the replacement was conceived by means of an easy-to-demount steel box supporting the pin, as illustrated in Fig. 1b. Moreover, in order to decrease the ovalization of the holes, the use of HSS for realizing the supporting boxes of the DRBrC components was foreseen.

3. Design of the prototype structure

In order to analyse the seismic performance of the DRBrC component in a full-scale structure, a prototype 3D six-storey building was designed. The building was characterized by a two-span CBF equipped with DRBrC components along the x-direction, and by a three-span MRF equipped with DRBeS components along the y-direction. Due to laboratory constraints, the span length was 4.275 m, while the inter-storey height was equal to 3.5 m. A concrete deck was connected by means of shear studs to the beams of the MRFs to develop the composite action in that direction. The structural seismic design was performed by means of linear dynamic analysis with response spectrum applied to a 3D finite element (FE) model developed in *SAP2000* [36]. The INNOSEIS provisions [24] were adopted for designing the dissipative replaceable components, while all the non-dissipative members were designed according to capacity design philosophy in accordance with European standards, i.e. EN 1993-1-1 [37], EN1993-1-8 [38], EN1994-1-1 [39] and EN 1998-1 [1]. Member profiles, DRBrC and DRBeS component dimensions are respectively reported in Tables 1–3. The deck was composed of a 150 mm high composite slab with a 55 mm high steel sheeting. An S355 steel grade was chosen for all the non-dissipative members. The supporting plates of the pin of the DRBrC components were made of either S355 (mild steel case) or S460 (HSS case). Finally, the DRBrC pin and the DRBeS plates were made of S235. Moreover, another 3D FE model was developed in *OpenSees* [40], in order to deeply investigate the nonlinear dynamic behaviour of the building and to investigate the substructured scheme needed to perform the HS tests. In this respect, linear beam-column elements were adopted for the beams, columns and braces, while nonlinear two-node links with *Pinching4* material were adopted for modelling both the dissipative components, i.e. the DRBrC and the DRBeS. In fact, a fully nonlinear model was not necessary as it was checked that the members did not undergo plastic behaviour and/or buckling. The parameters describing both the monotonic backbone curve and the hysteretic loops shape of the DRBrC were calibrated based on cyclic experimental curves obtained by IST Lisbon [41], whereas the ones describing the DRBeS behaviour were calibrated in accordance with Calado et al. [7,42]. The initial calibration procedure of the *OpenSees* constitutive models was performed by means of the software *Multical* [43] and the calibration

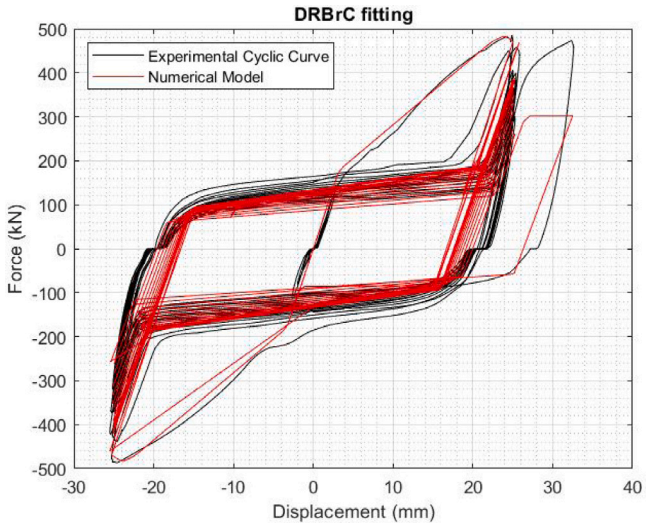

Fig. 2. Preliminary calibration of the DRBrC constitutive model in *OpenSees*.

Table 1
Columns and beams sections for six-storey building.

Floor	Element	Profile
1-2	Perimetral column	HE 260 B
3-4-5	Perimetral column	HE 240 B
6	Perimetral column	HE 220 B
1-2	Internal column	HE 300 B
3-4-5	Internal column	HE 280 B
6	Internal column	HE 260 B
1-2	Braces	HE 140 A
3-4-5	Braces	HE 120 A
6	Braces	HE 100 A
All floors	Beam MRF	IPE 270 + 150 mm composite deck
All floors	Beam CBF	IPE 300

Table 2
DRBrC component dimensions for the overall building. Dimensions in mm.

Floor	Pin diameter	Chamfering
1–2	45	5
3–4	40	5
5–6	35	5

of the DRBrC component is shown in Fig. 2. As it will be shown in more detail in Section 6, in the DRBrC components, the effect of the pin-plate clearance is not negligible and a gap material had to be put in series with the *Pinching4* model. The HS tests were carried out on a 2D frame equipped with DRBrC extracted from the 3D building. Since the displacement DoFs are easily controlled and the bending moment in continuous columns of CBFs is negligible, one actuator that controlled the horizontal displacement was applied to the PS at the level of the first floor. In this way, the PS consists of the first floor of the frame, while the remainder of the structure was included in the NS. The NS is nonlinear and includes the nonlinear modelling of the DRBrC components. For validating the different steps of modelling, i.e. 3D building, 2D frame and 2D substructured frame shown in Fig. 3, comparisons were performed in terms of modal, pushover and time-history analyses [44]. Fig. 3 shows the pushover curve comparison, while Table 4 reports the comparison in terms of the first four periods related to the mode of vibration in the DRBrC frame direction. From Fig. 3 and Table 4, it is possible to observe that good agreement between the models was achieved.

Moreover, the $P-\Delta$ effects were also investigated and relevant comparisons in terms of pushover and time-history analyses showed that they were negligible. In greater detail, pushover analyses on the 2D substructured frame were performed by also including the axial

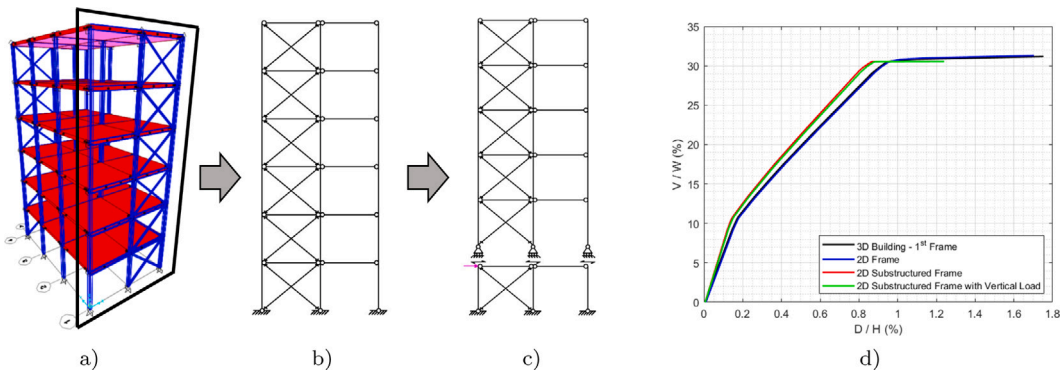

Fig. 3. Substructuring process of the prototype building: 3D Building (a), 2D Frame (b) and 2D Substructured Frame (c). Validation of the substructuring process by means of pushover analysis (d).

Table 3
DRBeS plates dimensions (width × thickness) for the overall building. Dimensions in mm.

Floor	Flange plate	Web plate
1–2–3	120 × 10	100 × 6
4	100 × 10	100 × 6
5–6	100 × 8	100 × 6

Table 4
Periods comparison for the three substructuring steps of modelling.

Mode	3D building T (s)	2D frame T (s)	2D Sub. frame T (s)
1	0.99	0.99	0.90
2	0.32	0.33	0.33
3	0.20	0.20	0.20
4	0.14	0.15	0.15

Table 5
Mechanical properties of S235 chamfered pins.

Property	Value
Yield strength f_y (MPa)	238.1
Ultimate strength f_u (MPa)	343.5
Elongation at failure (%)	37

load in the columns, and the results are shown in Fig. 3d. Indeed, no appreciable effect owing to the application of the vertical axial load can be observed. This was expected since CBFs are typically characterized by high lateral stiffness and second-order effects are, thus, negligible. Time-history analyses confirmed such results. Hence, since the application of vertical loads to the PS does not significantly affect the accuracy of the substructure, they were not applied to the columns of the PS.

4. Experimental test set-up

This section presents the design of the hybrid test set-up, as well as the instrumentation system applied to the specimens, namely the one equipped with DRBrC components with plates made of mild steel and the one equipped with DRBrC components with plates made of HSS. In this respect, Fig. 4 depicts the hybrid test configuration, while Fig. 5 shows the hybrid test set-up, comprising only the first floor of the frame. The frame consists of three 3.5 m high columns, two beams characterized by a span length of 4.275 m, and two bracing diagonals installed on the left span, as shown in Fig. 4. The profiles of the columns, i.e. HE 260 B, and of the braces, i.e. HE 140 A, were consistent with Table 1, whereas, in order to prevent buckling under compression action owing to the actuator force, the IPE 300 representing the beam was replaced with an HE 220 B. Note that such modification, has a marginal effect on the experimental frame dynamic behaviour, in terms of lateral stiffness of the bracing system. Moreover, it is to be noted that no concrete slab was included in the experimental specimen. This is because, in a CBF scheme, the beam-to-column joint is a simple hinge, and the beam is not subjected to flexure owing to seismic loading. Therefore, axial stiffness is dominant in the CBF behaviour when subject to horizontal forces. In this respect, the axial stiffness provided by the steel beam was high enough to transfer the horizontal loads without the need for the concrete part of the section, that for simplicity, was not included in the PS.

The DRBrC components were mounted at the end of each brace, as shown in Fig. 5. One brace was continuous, whereas the other was interrupted and the continuity was restored through two plates welded on the flanges. Moreover, the braces were installed in such a way as to have the weak axis in the plane of the bracing system. The mechanical properties of the S235 chamfered pins where the inelastic behaviour is expected are reported in Table 5. As previously mentioned, since the behaviour of the DRBrC depends on the axial forces in the braces, one actuator that controls the horizontal DoF located at the top of the ground floor suffices to well characterize the seismic behaviour of the components. Indeed, numerical analyses confirmed that there was no advantage in the employment of two actuators at different height levels. Finally, it is worth noting that the force read by the load cell mounted on the actuator represents the total shear at the base of the frame.

4.1. Instrumentation system

As depicted in Figs. 6a and b, instruments were employed to measure both local and global quantities. In greater detail, strain gauges were applied to the main members in the elastic parts of the structure, while displacement transducers were applied at the lateral sides of each DRBrC component and at the floor level on the right column in Fig. 4. To estimate the axial force acting on the DRBrC components, a couple of strain gauges was applied at the ends of each diagonal, as depicted in Fig. 7a. The strain measurements of the two flanges, i.e. ε_1 and ε_2, were then employed to respectively estimate the average strain and the axial force by means of the following formulas

$$\varepsilon_{avg} = \frac{\varepsilon_1 + \varepsilon_2}{2} \tag{1}$$

$$N = E_s \cdot A_s \cdot \varepsilon_{avg} \tag{2}$$

where E_s and A_s are Young's modulus of steel, assumed to be 210 GPa, and the cross-sectional area of the diagonal profile, respectively. The same procedure was employed to estimate the axial force in the beam. The relative displacement of the DRBrC components was obtained as

$$\Delta_{avg} = \frac{\Delta_1 + \Delta_2}{2} \tag{3}$$

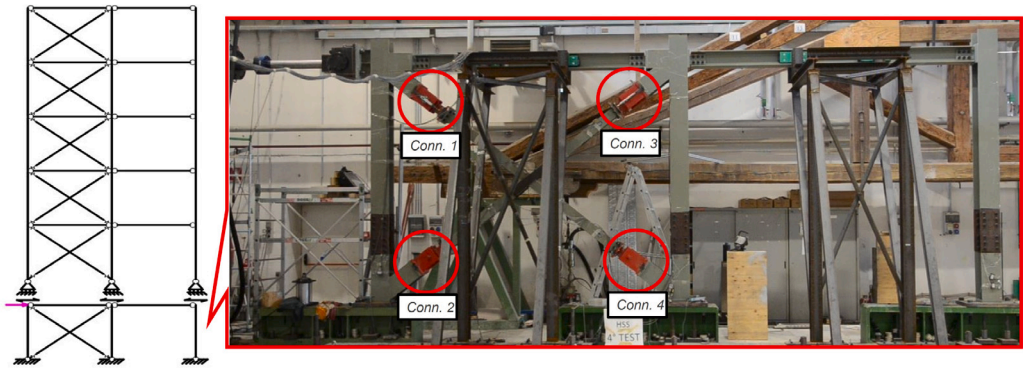

Fig. 4. Conception of hybrid test.

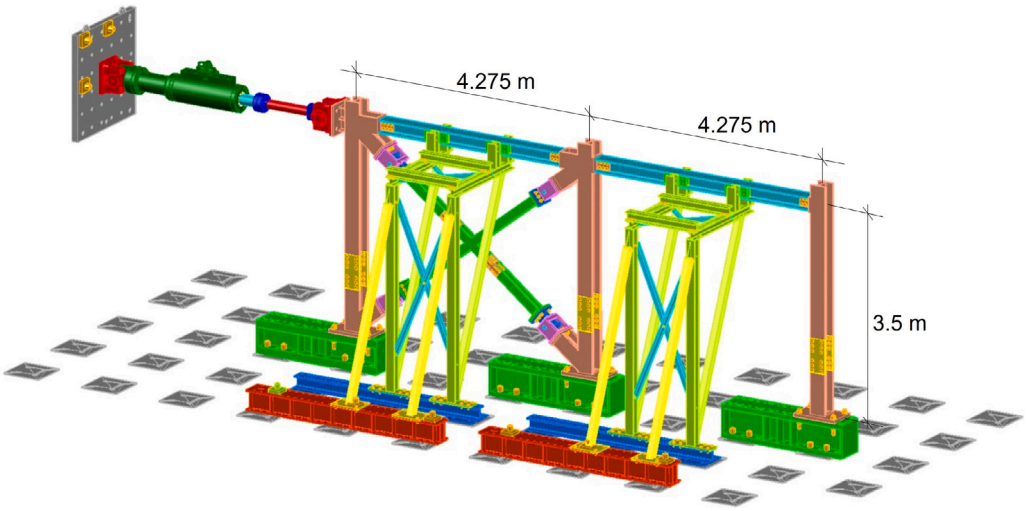

Fig. 5. Experimental specimen.

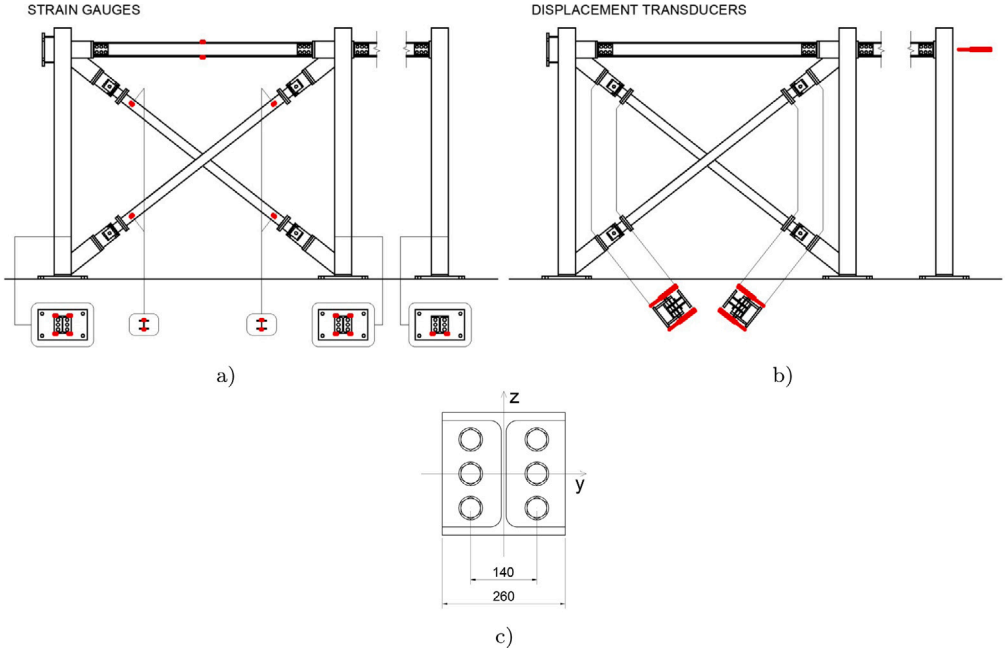

Fig. 6. Instruments configuration: (a) strain gauges applied on bracing diagonals, base columns and beam mid-span; (b) displacement transducers applied on the sides of the DRBrC connections; (c) plan section of the base column connection (HE 260 B).

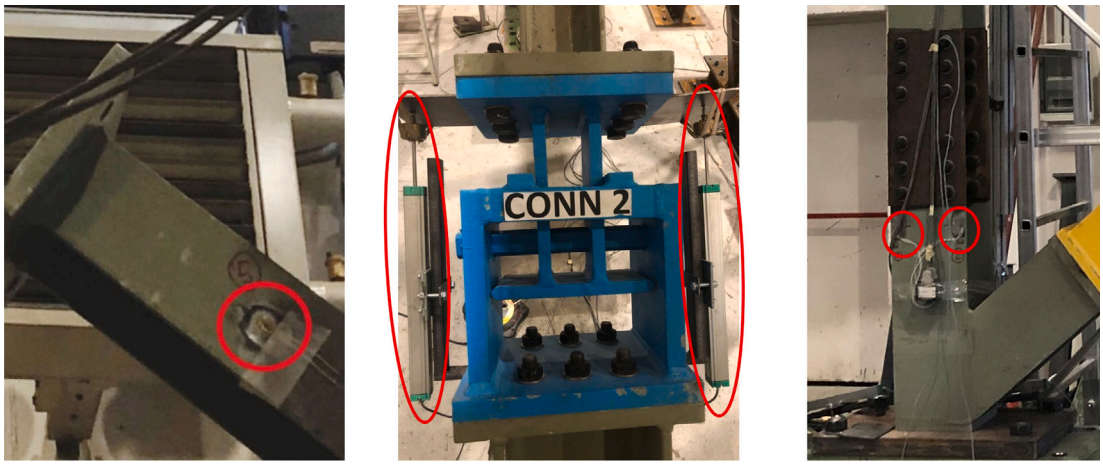

Fig. 7. Pictures of the different instruments employed in the test: (a) strain gauge on brace, (b) displacement transducers of DRBrC component and (c) strain gauges on column.

where Δ_1 and Δ_2 are the measurements recorded from the displacement transducers on the sides of the DRBrC component, depicted in Fig. 6b. Since the column bases cannot be regarded as perfect hinges, see Fig. 6c, to predict any possible bending action at the base of the frame, strain gauges were applied at the column bases, as shown in Fig. 7c. Then, the curvature at the base was estimated as

$$\chi_i = \frac{\varepsilon_{i,left} - \varepsilon_{i,right}}{B_{sec}} \tag{4}$$

where $\varepsilon_{i,left}$ and $\varepsilon_{i,right}$ are the strain gauge measurements at the left and right edges of the ith profile flange, while B_{sec} is the profile width. The bending moment estimate could then be obtained from linear-elastic assumptions:

$$M_i = E_s I_z \chi_i \tag{5}$$

$$M = average(M_i) \tag{6}$$

where I_z is the profile inertia moment with respect to the weak axis. Finally, in order to evaluate the rotational stiffness $S_{j.ini} = M_i/\phi_{chord}$ of the column bases, the chord rotation was estimated through the column top displacement Δ_{col}, as

$$\phi_{chord} = \frac{\Delta_{col}}{H_{col}} \tag{7}$$

where the column height H_{col} is equal to 3.5 m, while the Δ_{col} was considered differently for each column, i.e. the actuator displacement feedback for the left column, the displacement transducer measurement for the right column and the average of these two for the central column.

5. Test program and ground motion selection

The frame was subjected to three different ground motions of increasing intensity that corresponded to, respectively, the Damage Limitation (DL), Significant Damage (SD) and Near Collapse (NC) limit states. To investigate the seismic response of the full-scale frame equipped with DRBrC components through HSs, the following test procedure was adopted:

1. Test at the DL limit state, after which the elastic behaviour of all dissipative devices and the structural members was checked.
2. Test at the SD limit state, after which the inelastic behaviour of the dissipative components and the elastic behaviour of the non-dissipative members were checked.
3. The damaged DRBrC components were then replaced with new ones.
4. Test at the NC limit state.

This procedure was adopted for both frames equipped with mild steel and HSS DRBrC components. Each of the three aforementioned HS tests was performed by giving as input an earthquake record, whose identification is, in general terms, not trivial. Hence, an accelerogram selection procedure was required to choose the best candidate for each limit state. To this aim, for each limit state, a suite of seven natural ground motions was selected. In particular, the selection of the horizontal component to be used in the HS tests was performed by means of two main criteria: spectral compatibility and minimization of the discrepancy between the monolithic and the substructured 2D frames. The first criterion was checked by means of the spectral compatibility requirements imposed by EN1998-1C8 [45] on the geometric mean of the two horizontal spectral acceleration components, defined as

$$GM = \sqrt{S_{e,X} \cdot S_{e,Y}} \tag{8}$$

where $S_{e,X}$ and $S_{e,Y}$ are the X and Y spectral acceleration components of the ground motion. The spectral compatibility requirements are herein briefly described:

- The compatibility is checked in the period ranges $[0.2T_{1x} - 1.5T_{1x}]$ and $[0.2T_{1y} - 1.5T_{1y}]$, being T_{1x} and T_{1y} the fundamental periods of the 3D building along the two main directions.
- In these ranges, the average of the 5% damped GM response spectra shall fall between 0.75 and 1.3 times the target spectrum, considered as the elastic spectrum defined by EN 1998-1C8.
- In the same ranges, the average value of the ratio between the average of the GMs and the target spectrum shall be greater than 0.95.
- In the same ranges, the 5% damped GM response spectrum of each accelerogram shall not fall below 50% of the target spectrum.

The records for which the aforementioned requirements are not met shall be scaled accordingly. In Fig. 8, $T_{min} = \min(T_{1x}, T_{1y})$ and $T_{max} = \max(T_{1x}, T_{1y})$. The third point of the aforementioned requirements is fulfilled given that the average value of the $\frac{meanGM}{S_e}$ ratio assumes the values of 1.00, 1.02 and 1.19 for the DL, SD and NC limit states, respectively. Fig. 8 shows the GM spectra related to the selected records, superimposing the limits prescribed by EN1998-1C8. Note that the requirements on spectral compatibility are fully met for the accelerograms at the DL and SD limit states, as depicted in Fig. 8a and b, while they are not for the NC limit state, see Fig. 8c. This happens because the latter is characterized by a pulse-like motion with larger spectral ordinate components for longer periods. Nevertheless,

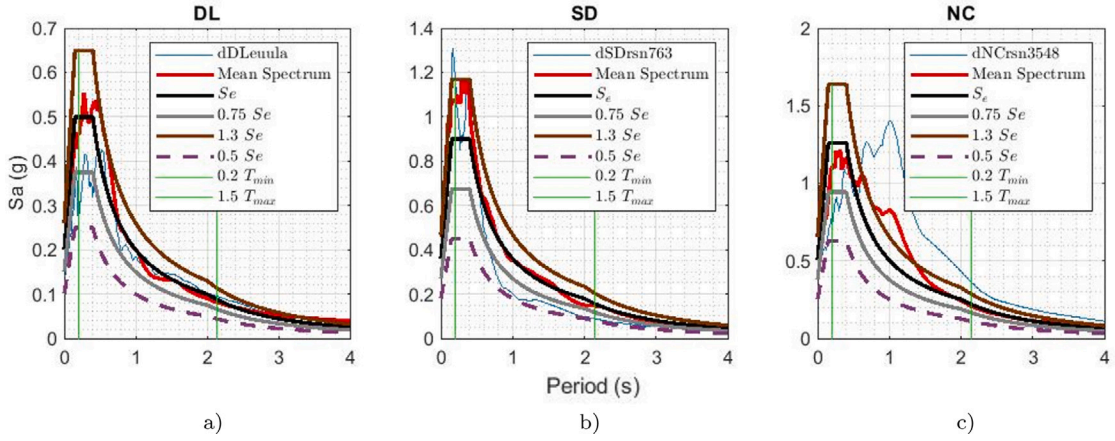

Fig. 8. Response spectrum of the selected accelerograms for (a) DL, (b) SD and (c) NC limit states and limits given from EN1998-1C8 for spectral compatibility.

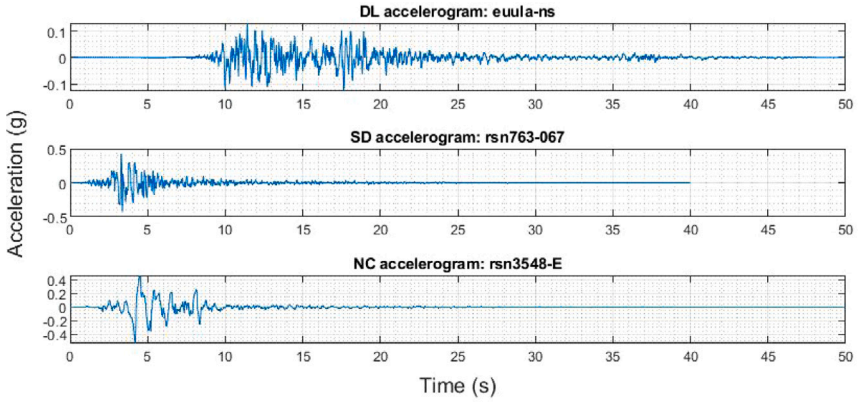

Fig. 9. Records selected for the tests at DL, SD and NC limit state.

Table 6
Parameters of error between monolithic and substructured frame responses. Errors are given in percentage (%).

Parameters	DL	SD	NC
NRMSE - Base shear V_{base}	7.58	4.02	3.96
NENERR - Base shear V_{base}	12.17	0.93	4.73
NRMSE - Axial Force 1st Floor Connections	8.23	4.68	2.09
NENERR - Axial Force 1st Floor Connections	11.20	6.14	5.24
NRMSE - Displacement 1st Floor	7.07	3.80	1.88
NENERR - Displacement 1st Floor	4.42	7.70	1.46

EN1998-1C8 [45] allows for the employment of such accelerograms, which indeed were exploited to obtain higher structural damage than for tests at the SD limit state.

Regarding the second criterion for selecting the record to be employed in the tests, the discrepancy between the 2D monolithic frame and the 2D substructured frame was quantified by considering the following parameters

$$NRMSE(\%) = \frac{\|x_i - x_j\|_2/\sqrt{N}}{x_{j,max} - x_{j,min}} \cdot 100 \tag{9a}$$

$$NENERR(\%) = \left| \frac{\|x_i\|_2 - \|x_j\|_2}{\|x_j\|_2} \right| \cdot 100 \tag{9b}$$

The parameters reported in Eqs. (9a) and (9b) compare two datasets, where j is the reference dataset. For the selection of the best record candidate at each limit state, the NRMSE and NENERR errors were computed for different meaningful quantities:

- the total base shear history
- the axial force history in the DRBrC components at the first floor
- the horizontal displacement history of the first floor

For each limit state, Table 6 reports the aforementioned error values in percentage. As shown, the monolithic and substructured 2D frame responses are in reasonable agreement, being the errors related to the DL limit state lower than 15% and the errors related to SD and NC limit states lower than 10%. Finally, Fig. 9 depicts the three different records employed in the HS tests.

6. Partitioned algorithm and model calibration for HSs

6.1. Partitioned algorithm

This section is devoted to briefly describing the numerical method used to perform the HS tests. The experimental HS tests were conducted by means of a partitioned algorithm based on the finite element tearing and interconnecting (FETI) method [46]. A $G-\alpha$ algorithm, previously developed by Abbiati et al. [47], was employed to simultaneously obtain the step-by-step equation of motion (EoM) solution for both the numerical and the physical subdomains. In brief, after rewriting both NS and PS systems of EoM in the state space form, the solutions are separately obtained for each subdomain. Then, they are coupled at each time step by imposing the compatibility conditions at the interface DOFs through Lagrange multipliers, resulting in the following coupled system of equations

$$\begin{cases} M^N \dot{Y}^N_{n+1} + R^N(Y^N_{n+1}) = L^N \Lambda_{n+1} + F^N_{n+1} \\ M^P \dot{Y}^P_{n+1} + R^P(Y^P_{n+1}) = L^P \Lambda_{n+1} + F^P_{n+1} \end{cases} \tag{10}$$

$$G^N \dot{Y}^N_{n+1} + G^P \dot{Y}^P_{n+1} = 0 \tag{11}$$

where M, R, and F are respectively the mass matrix, restoring force vector and load vector written in the state space form [47], whereas Λ_{n+1} is the Lagrange multiplier that, in this case, assumes the physical meaning of a force. L and G are boolean collocation matrices that respectively localize the interface forces and define compatibility, being the latter expressed in Eq. (11) by means of the first derivative of the state vector, $\dot{Y}$. The apexes ^{N} and ^{P} are respectively related to numerical and PS matrices and vectors. In Eq. (10), the vector R contains both the PS restoring force, obtained by the measurement of the actuator load cell, and the NS restoring force, that, in the linear case, reduces to the algebraic product of the stiffness matrix times the displacement vector, both written in the state space form. Nonetheless, all DRBrC components part of the NS were included by means of nonlinear elements, for which the restoring force was computed separately by an ad-hoc *Pinching4* routine implemented for the purpose. Only one horizontal degree of freedom was controlled in the physical specimen. Therefore, the PS computational model had to be condensed into a single-degree-of-freedom (SDOF) model. The component mode synthesis method was adopted to reduce the size of the stiffness matrix to a scalar number [48,49]. Here, the reduced-order component $\hat{u}$, is obtained as:

$$\hat{u} = \hat{\Psi} \hat{p} \tag{12}$$

where $\hat{\Psi}$ is the component mode matrix and $\hat{p}$ is the generalized coordinate vector. The NS restoring force vector in Eq. (10) included the viscous damping contribution, while the PS damping is considered to be inherently included in the physical specimen, and therefore set to zero in the algorithm. The HSs were performed as pseudodynamic tests; hence, a time-scaling factor λ was adopted for expanding the time scale.

$$\lambda = \frac{\Delta t_C}{\Delta t} \tag{13}$$

In Eq. (13) Δt_C and Δt are respectively the time integration step used for solving the equation of motion and the wall clock time that marks the solution of a one-time integration step. Since the mass contribution was numerically simulated for both PS and NS, to assure that no residual inertial forces were included in the tests, the time scaling factor had to be set to a sufficiently high value that was chosen equal to $\lambda = 50$ for the DL limit state and $\lambda = 100$ for the SD and NC limit states.

6.2. Model calibration

The inclusion of nonlinear elements in the NS requires the estimation of the related nonlinear parameters, which in general terms it is not a trivial task. As described in Section 3, the *Pinching4* parameters describing the backbone monotonic curve were initially computed by following the INNOSEIS formulation [24], and then re-calibrated by fitting the experimental cyclic curves provided by IST Lisbon [41]. In doing so, the behaviour of the two-node link representing the DRBrC component was assumed to be linear at least in the elastic range. After performing preliminary cyclic tests on the physical frame, it was clear that the assumption of a linear DRBrC constitutive law could not be regarded as valid even in the elastic range, where no damage and dissipation take place. Indeed, a non-negligible gap-clearance slip was detected between the pin and the eyebar plate hole, introducing a substantial discrepancy with the FE model.

This discrepancy highlighted the need for a new calibration of the DRBrC component constitutive law, that could account for this type of nonlinearity. An additional issue in reproducing the mechanical behaviour of the DRBrC components was related to the gap amplitude and the position of the pin in the hole with respect to the central point, whose values are intrinsically random by nature and, therefore, different for each connection. Because of this, the new constitutive law parameters were obtained first by fitting the force–displacement behaviour of the four connections, and then by averaging the four sets of parameters. As a result, a trilinear constitutive law was conceived for modelling the connection elastic behaviour, i.e. (i) a branch of very low stiffness representing the pin slip with the gap estimated as ± 0.5 mm; (ii) a linear branch representing the behaviour in tension and (iii) a linear branch representing the behaviour in compression, which were both described by the same value of elastic stiffness, as reported in Table 7. The axial force–displacement diagrams of the physical DRBrC components related to the preliminary cyclic tests are shown in Fig. 10, where the stiffnesses related to the three different calibrations of the DRBrC constitutive relationship are superimposed and compared. Table 7 reports the values of elastic stiffness related to the different constitutive laws for the DRBrC component. Note that the DRBrC stiffness originally calculated by following the INNOSEIS provisions was reduced after the first calibration with Multical (see Fig. 2) of the experimental cyclic curves provided by IST Lisbon [41], because its value inherently includes the approximated effect of the pin clearance. Conversely, the post-gap stiffness in the trilinear constitutive law essentially validates the original stiffness of the INNOSEIS formulation, which does not account for the gap-clearance. From the numerical point of view, in the *OpenSees* reference model the gap-like behaviour was included by adding an *ElasticPerfectlyPlasticGap* material in series to the *Pinching4* material. In contrast, for the numerical part of the HS test, the gap effect was obtained by appropriately modifying the algorithm for computing the nonlinear restoring force. Moreover, the DRBrC components were replaced between SD and NC tests of both mild steel and HSS experimental test campaigns, resulting in four different sets of connections, see the assigned colour in Table 8, and each of them characterized by a different average gap clearance. Hence, for each set of connections, it was necessary to quantify the average gap clearance and estimate the stiffness value of the PS to adopt in the algorithm. In order to do so, after mounting each set of new connections, a preliminary HS test was performed with the DL limit state accelerogram, scaled by a coefficient equal to 0.3. In this respect, for each set of DRBrC components, the force–displacement feedback of the actuator is shown in Fig. 11. Finally, another clear outcome obtained by the preliminary cyclic tests is the existence of a non-negligible rotational stiffness at the column base joint, as previously mentioned in Section 4. This aspect introduced a further discrepancy with the original braced frame model, as highlighted by the experimental results presented in Section 7. Thus, the value of the column base joint rotational stiffness was experimentally estimated by means of the strain gauge and the actuator displacement measurements, which allowed for an estimation of the moment-rotation diagram according to elastic theory. As a result, the rotational stiffness of the base joint was found equal to 14.8 kN m/mrad, and was included through a linear link at the base of the columns in both the PS model for the HSs and in the *OpenSees* reference model.

Table 7
Elastic stiffness of the DRBrC.

Property	K (kN/mm)
INNOSEIS	83.07
Preliminary calibration	44.19
Trilinear - post gap tension and compression	73.71
Trilinear - gap	1.30

Table 8
DRBrC colour for each test.

Test	Mild steel	HSS
DL	Green pin	Yellow pin
SD	Green pin	Yellow pin
NC	Blue pin	Red pin

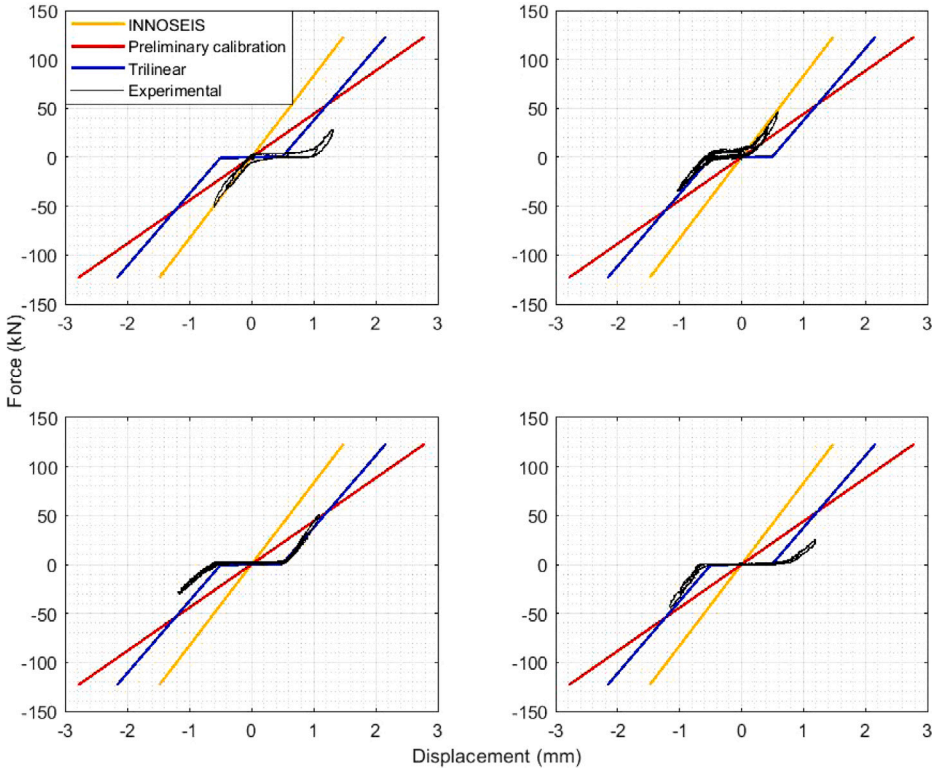

Fig. 10. DRBrC stiffness calibrations.

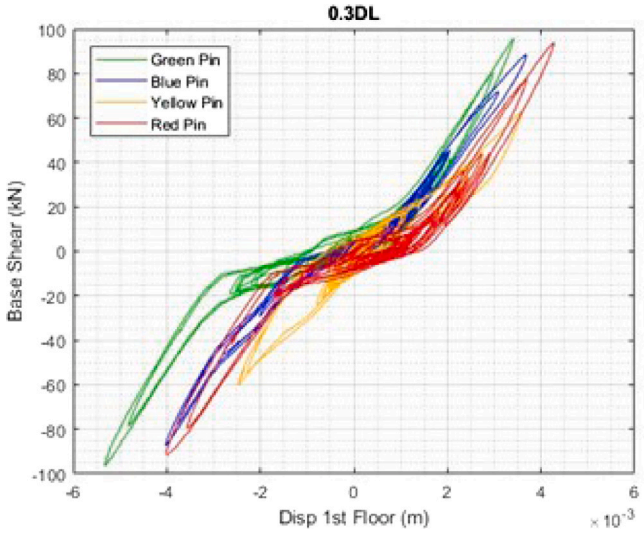

Fig. 11. Actuators feedback for the different sets of DRBrC components - input: 0.3 DL accelerogram.

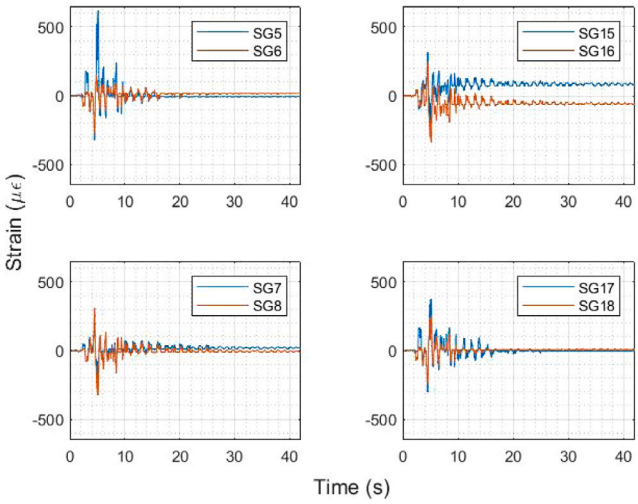

Fig. 12. Braces strain gauges acquisition history for NC test. Yield deformation ε_y = 1690 με.

7. HS results

In this section, the main experimental results for the frame equipped with mild steel DRBrC components are described. Afterwards, the main differences between the outcomes obtained with mild steel and HSS supporting plates will be compared.

It is important to note that, for all the limit states, the strain gauges applied to the braces measured strain values in the elastic range, as shown by Fig. 12 for the NC case, and no buckling phenomena were observed. This is highly beneficial for the repairability of a steel frame equipped with DRBrC components. Herein, the figures representing the behaviour of the four physical DRBrC components, follow the order reported in Fig. 4.

7.1. DL limit state

Fig. 13 depicts the axial force–displacement diagram of each physical DRBrC component, where a positive ordinate means compression force. Significant pinching effect and slip at zero force level can be noticed, which are assumed to be due to the hole clearance in the pinned connection, which confirms what is discussed in Section 6.

Moreover, small hysteretic behaviour was detected even at the DL limit state, which was instead expected to be negligible from the

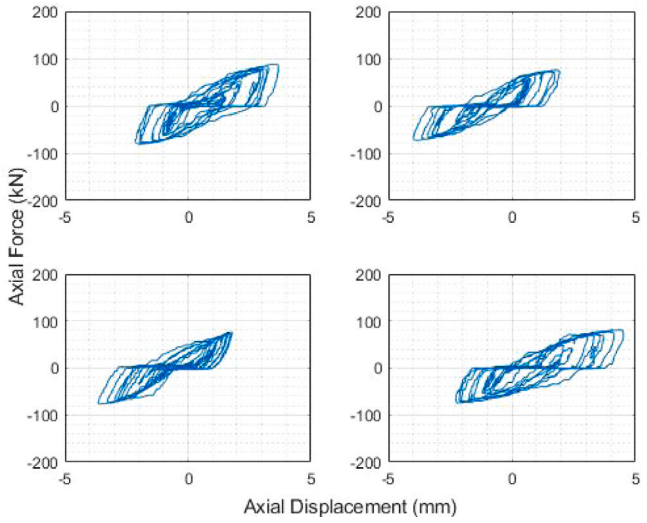

Fig. 13. DL - Experimental axial force–displacement diagrams of DRBrC components.

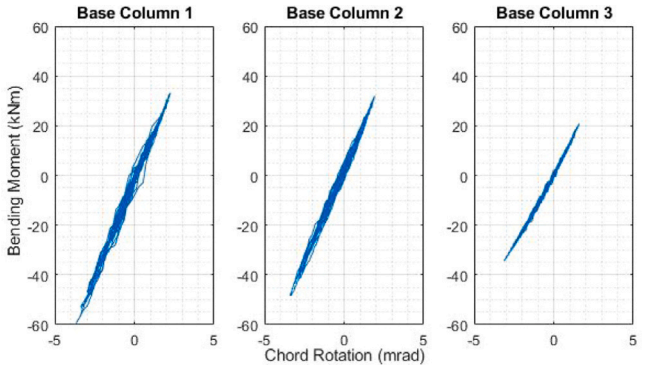

Fig. 14. DL - Experimental moment-rotation diagrams of column bases.

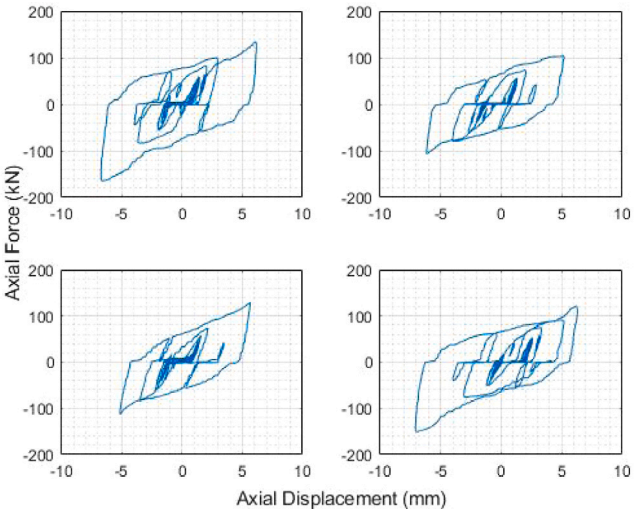

Fig. 15. SD - Experimental axial force–displacement diagrams of DRBrC components.

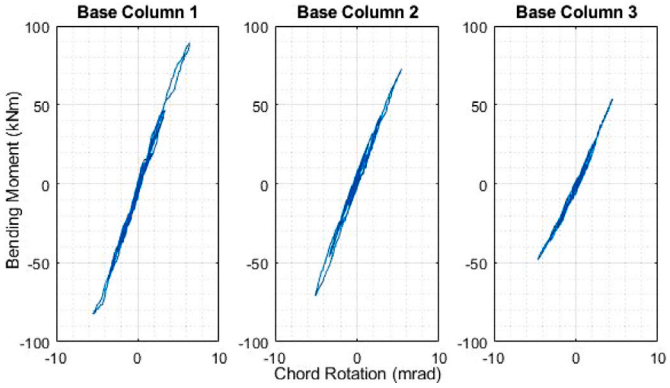

Fig. 16. SD - Experimental moment-rotation diagrams of column bases.

Fig. 17. SD - Pin Extraction after SD test.

reference model. This may be due to the fact that the reference model does not account for the local bearing of the pin that was made of steel grade S235. As described in Section 4, strain gauges were employed to estimate the bending actions at the column bases. In this respect, substantial bending moments were predicted at each column base, as shown in Fig. 14. Nevertheless, linear behaviour was observed, which excludes any plastic behaviour of column bases at the DL limit state.

7.2. SD limit state

Fig. 15 shows the axial force–displacement diagram of each physical DRBrC component.

A favourable hysteretic dissipation with large loops was exhibited by the DRBrC components with significant pinching caused by the pin-hole clearance and the bearing of the plates and of the pin. As for the DL limit state test, strain gauges were employed to estimate the bending moment at the column bases, which is depicted in Fig. 16 against the column chord rotation. A linear behaviour was observed, which excludes the occurrence of damage and plastic deformation in the column bases, that demonstrate the effective capability of the DRBrC components to protect the irreplaceable members. As mentioned in Section 5, in order to verify the repairability of the frame, the damaged DRBrC components were replaced after the SD limit state test. The practical replacement of the DRBrC components was performed through the following main steps:

1. One component at one time was removed.
2. The bolts were unscrewed and removed.
3. The damaged DRBrC component was removed by pushing it in the out-of-plane direction. A crane was used to lift and hold the component.
4. A new DRBrC component was inserted in the same position.
5. A new set of bolts was inserted and screwed in.

No particular issues were encountered in substituting the DRBrC components. An interesting outcome was the possibility of extracting the pin from the box after the SD limit state test without much effort,

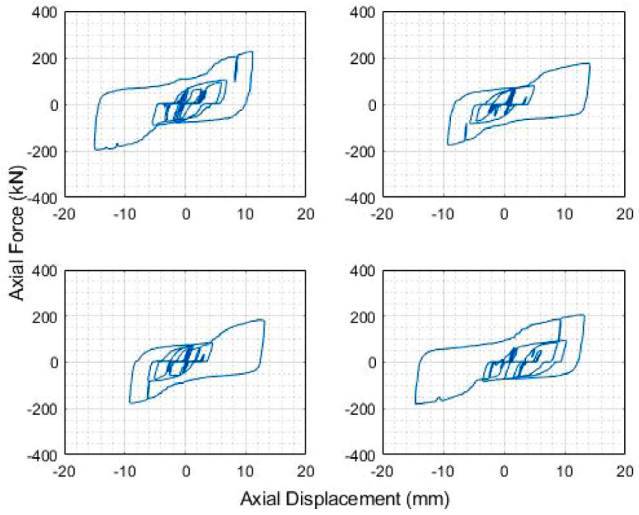

Fig. 18. NC - Experimental axial force–displacement diagrams of DRBrC components.

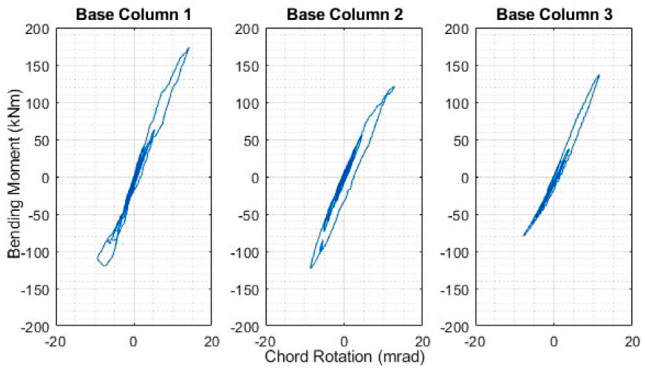

Fig. 19. NC - Experimental moment-rotation diagrams of column bases.

as shown in Fig. 17. This was observed both for the mild steel and HSS tests. This is a positive outcome also in the context of residual displacements and re-centring capabilities, as reported in Table 9.

7.3. NC limit state

Fig. 18 shows the axial force–displacement diagram of the four physical DRBrC components. Significant dissipation capability due to a large nonlinear behaviour of the DRBrC components under NC limit state actions can be observed. Displacements up to 15 mm were detected without failure of the components. Higher pinching effect than the SD limit state case appeared, which is due to the large displacement of the pin, as well as the larger forces and consequent larger bearing of the pin. As shown in Table 9, very small residual displacements were observed which enhance the self-centring capabilities and quicker repairability. Furthermore, a satisfactory comparison in terms of components axial force–displacement diagrams is obtained between the HS test and the reference model, which is reported in Fig. 20 both for the PS and the NS.

Bending moments at the column bases are depicted in Fig. 19, where a linear behaviour is highlighted, that demonstrates how the DRBrC components are able to efficiently protect the irreplaceable parts even at the NC limit state. Fig. 21 shows the comparison, in terms of Base shear vs. Top floor displacement graph between the HS test and the *OpenSees* reference model, where the pushover curve obtained from *OpenSees* is superimposed. A satisfactory agreement between the experimental HS data and the reference model can be observed for all tests at the different limit states. Yielding was slightly approached for the DL limit state test, demonstrating the elastic behaviour of the frame throughout the test.

Conversely, for SD and NC limit state tests, yielding was exceeded, resulting in wide hysteretic energy dissipation in particular for the NC limit state.

Table 9
Residual actuator displacement and interstorey drift after DL, SD and NC limit state tests for both Mild steel and HSS cases.

Specimen	DL	SD	NC
Mild steel	1.2 mm (0.4‰)	0.1 mm (0.0‰)	0.6 mm (0.2‰)
HSS	1.3 mm (0.4‰)	1.7 mm (0.5‰)	6.1 mm (1.7‰)

7.4. Comparison between Mild Steel vs. HSS

The comparison between mild steel and HSS DRBrC components is performed in terms of axial force–displacement cycles, as shown in Figs. 22, 23 and 24 for DL, SD and NC limit state tests, respectively. From the figures, one may observe that in some cases the diagram, that characterized the behaviour of the DRBrC component made of mild steel, is shifted to the left or to the right with respect to the one made of HSS, as for the DRBrC component at the bottom left for the DL and the SD limit states (see Figs. 22 and 23). This is due to the inherent randomness of the clearance between the hole and the pin along with the position of the pin within the hole at the start of the test. Indeed, the main discrepancies in the comparison of the axial force–displacement diagrams between mild and HSS DRBrCs were mainly caused by these construction details. In this respect, it is worth pointing out that when the DRBrC component at the bottom left was replaced with a new one to perform the test at the NC limit state, such a large shift in the diagram was not observed anymore, as shown in Fig. 24. With regard to strength, stiffness and dissipative capacity, no major differences were observed when the supporting plates of the pin were made of HSS. This is in partial contrast with what is reported in [24] and in [41] for the tests performed at IST, because the tests in [24] and in [41] were performed according to the ECCS testing protocol [50], which is typically more severe with respect to a test conducted with an actual accelerogram and the ECCS testing protocol was directly applied to the single component. Indeed, the ECCS testing protocol is generally used to assess the capacity of a component, whereas the tests performed in the context of the DISSIPABLE project aimed at assessing the performance of the structural system. As a result, the maximum displacements exhibited in the HS tests were not large enough to mobilize the beneficial effects of higher steel grade [41]. Moreover, also the residual displacements were similarly very small (see Table 9). Finally, Fig. 25 reports the deformation state of the DRBrC components at the peak response of the SD and NC tests. It is possible to observe a clear inelastic behaviour of the pin.

8. Conclusions

The article extensively presented the results of a large experimental campaign performed on a full-scale steel-braced frame equipped with DRBrC components. By performing tests at different levels of seismic intensity, i.e. DL, SD and NC limit states, it was possible to comprehensively characterize the frame behaviour in the elastic and inelastic fields. The possibility of repairing the frame by replacing the dissipative components was demonstrated. The main outcomes of the overall test campaign are reported below:

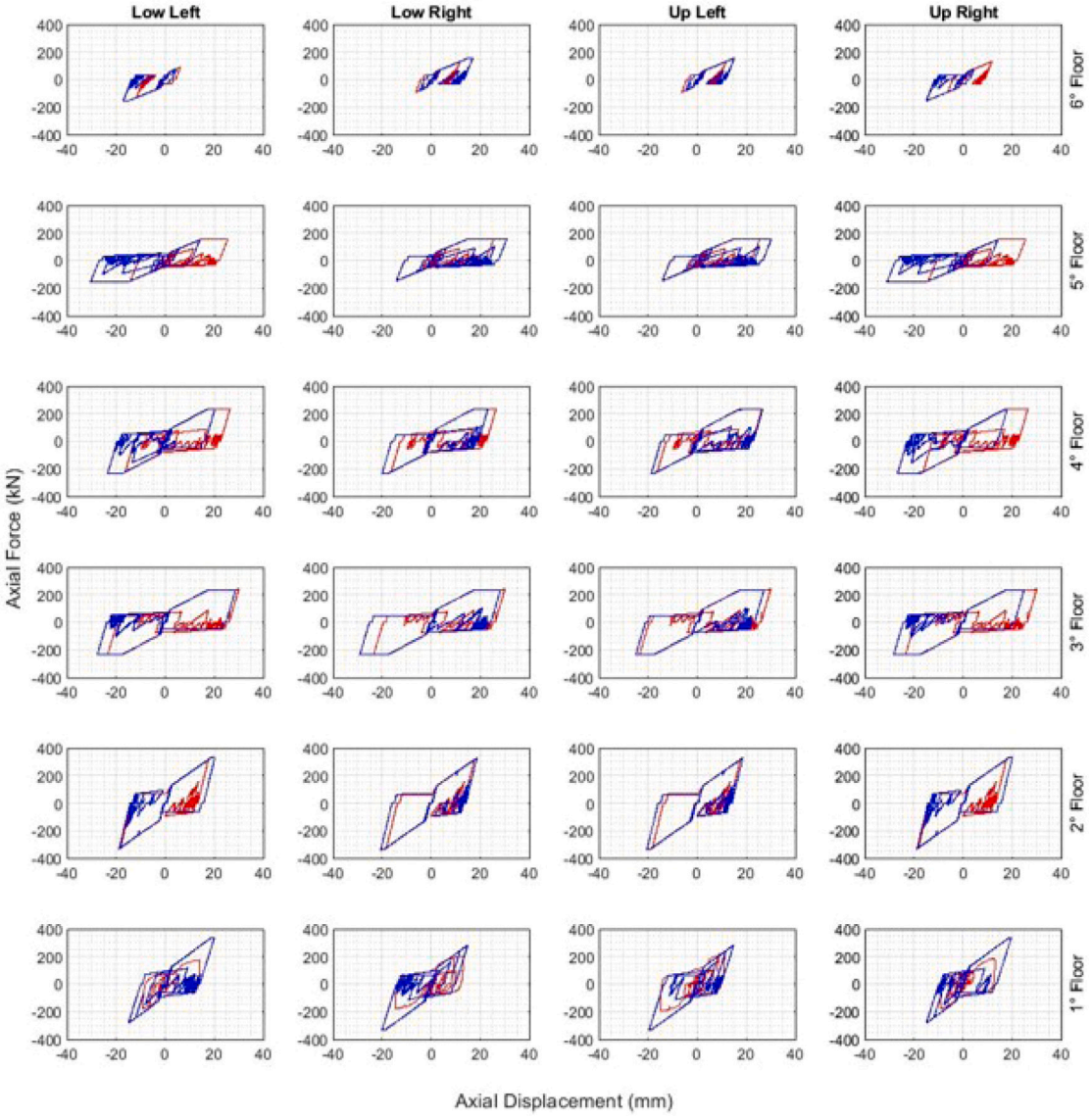

Fig. 20. NC - Comparison of axial force–displacement diagrams of DRBrC components for physical and numerical subdomains between HS, in red, and OpenSees reference model, in blue.

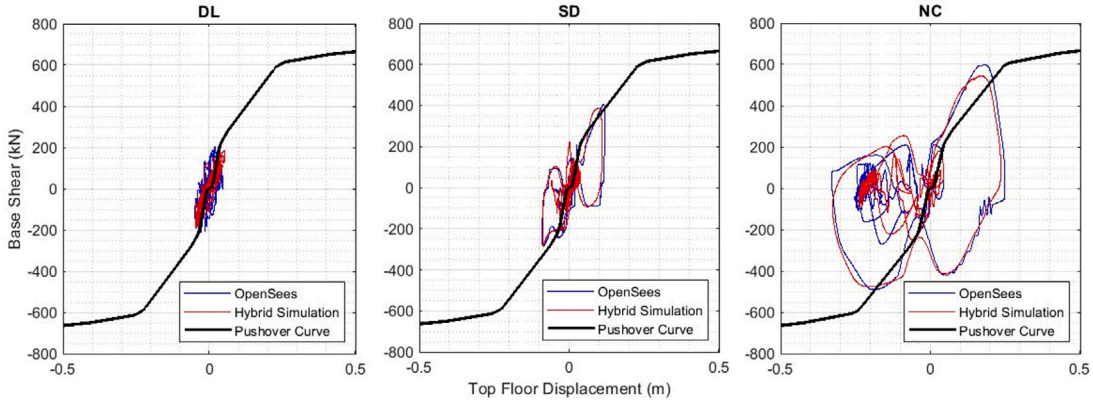

Fig. 21. Comparison of Base shear vs. Top floor displacement diagrams between hybrid test and reference model - DL, SD and NC limit states.

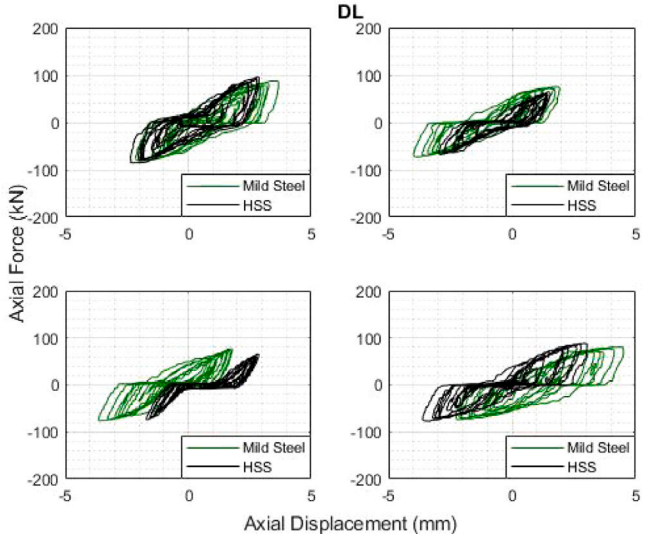

Fig. 22. DL - Superposition of mild steel and HSS DRBrC axial force–displacement diagrams.

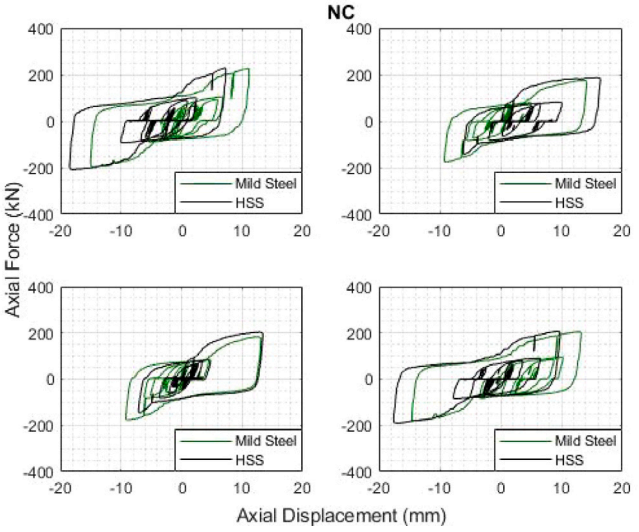

Fig. 24. NC - Superposition of mild steel and HSS DRBrC axial force–displacement diagrams.

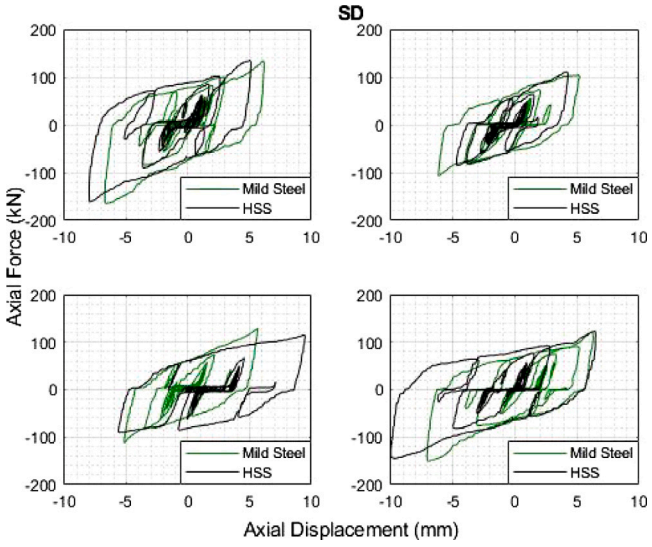

Fig. 23. SD - Superposition of mild steel and HSS DRBrC axial force–displacement diagrams.

components highlighted a favourable hysteretic behaviour with large loops owing to the pin inelastic behaviour both in bending and shear. For all tests, a substantial pinching effect was detected. The three main sources of this phenomenon are (i) the pin-hole clearance, (ii) the pin local bearing and (iii) the hole ovalization. Moreover, for the NC limit state test, the large deformation of the pin caused an increment of the pinching phenomenon.

- A non-negligible clearance, about 1 mm, was detected in the physical DRBrC components between the pin and the eyebar plate hole, which affected the dynamic behaviour of the connections and the overall frame. For consistency between PS and NS, this clearance was included in the numerical part of the frame by appropriately modifying the algorithm that includes a gap-like behaviour in the nonlinear DRBrC elements.
- The non-dissipative parts of the frame, i.e. braces, columns and beams, did not experience inelastic behaviour at any limit state test, which proves the good performance of the DRBrC components in protecting the irreplaceable parts of the frame even for ground motion intensities larger, i.e. NC limit state, than the design one, i.e. SD limit state. Moreover, at each limit state, small residual displacements were observed that enhanced the self-centring capabilities and the repairability of the CBF equipped with DRBrC components. Indeed, the connections could be replaced after the tests at the SD limit state without particular effort, highlighting an optimal performance of the DRBrC components in the context of enhanced structural seismic resilience and the PBEE approach.
- No significant improvements or differences in the seismic performance of DRBrC components made with HSS supporting plates were found because the maximum displacements were not large enough to show the beneficial effects of a higher steel grade.

Overall, the steel CBF equipped with DRBrC components exhibited favourable under seismic action by guaranteeing at the same time large dissipation and repairability capabilities. As a future perspective, design provisions for DRBrC components that account for the effect of the internal slip due to the pin-hole clearance into the global deformability checks should be developed. This would help practitioner engineers include such devices in common practice design without running non-linear time-history analyses. Moreover, the DRBrC components could be used as a retrofit measure within an external exoskeleton.

- The HS technique, through the implementation of the partitioned $G-\alpha$ algorithm, was successfully employed. It allowed to reliably reproduce the dynamic response of the overall frame, including the five storeys above the one built in the laboratory. Moreover, by means of the HS technique, it was possible to assess the ability of the DRBrC components to dissipate large amounts of energy by protecting the non-dissipative members through full-scale tests without the need to scale down the structural geometry. Thus, it was also possible to limit the overall costs of the experimental tests.
- The seismic loading was realistically replicated, and the structure was tested at different limit states. In particular, at the DL limit state the structure basically underwent elastic behaviour of the connections, with a small hysteretic dissipation due to the local bearing of the pin. At the SD and NC limit state, the DRBrC

Fig. 25. DRBrC component number 2 during peak response at SD and NC limit states, for both mild steel and HSS components.

CRediT authorship contribution statement

Roberto Andreotti: Methodology, Software, Validation, Data processing, Writing – original draft. **Giulia Giuliani:** Methodology, Software, Data processing, Writing – review & editing. **Nicola Tondini:** Conceptualization, Methodology, Supervision, Writing – review & editing, Funding acquisition.

Declaration of competing interest

The authors declare the following financial interests/personal relationships which may be considered as potential competing interests: Nicola Tondini reports financial support was provided by Research Fund for Coal and Steel.

Data availability

Data will be made available on request.

Acknowledgements

This project has received funding from the Research Fund for Coal and Steel under grant agreement No 800699. Views and opinions expressed are however those of the author(s) only and do not necessarily reflect those of the European Union or Research Fund for Coal and Steel. Neither the European Union nor the Research Fund for Coal and Steel can be held responsible for them. The research leading to these results has also received funding from the Italian Ministry of Education, Universities and Research (MUR) in the framework of the project DICAM-EXC (Departments of Excellence 2023–2027, grant L232/2016)

References

[1] CEN, EN 1998-1 - Eurocode 8: Design of Structures for Earthquake Resistance - Part 1: General Rules, Seismic Actions and Rules for Buildings, CEN - European Committee of Standardization, Bruxelles, 2004.
[2] J. McConnell, L. Fahnestock, Innovation in steel design: Research needs for global sustainability, J. Struct. Eng. 141 (2015) http://dx.doi.org/10.1061/(ASCE)ST.1943-541X.0001185.
[3] R. Pucinotti, N. Tondini, G. Zanon, O. Bursi, Tests and model calibration of high-strength steel tubular beam-to-column and column-base composite joints for moment-resisting structures, Earthq. Eng. Struct. Dyn. 44 (2015) 1471–1493.
[4] N. Tondini, G. Zanon, R. Pucinotti, R. Di Filippo, O. Bursi, Seismic performance and fragility functions of a 3D steel-concrete composite structure made of high-strength steel, Eng. Struct. 174 (2018) 373–383, http://dx.doi.org/10.1016/j.engstruct.2018.07.026.
[5] J. Castro, A. Elghazouli, I. B.A., Modelling of the panel zone in steel and composite moment frames, Eng. Struct. 27 (2005) 129–144.
[6] R. Montuori, E. Nastri, V. Piluso, M. Troisi, Influence of connection typology on seismic response of MR-frames with and without 'set-backs', Earthq. Eng. Struct. Dyn. 46 (2017) 5–25.
[7] R. Andreotti, G. Giuliani, N. Tondini, O. Bursi, Hybrid simulation of a partial-strength steel-concrete composite moment-resisting frame endowed with hysteretic replaceable beam splices, Earthq. Eng. Struct. Dyn. (2022) http://dx.doi.org/10.1002/eqe.3744.
[8] G. Vasdravellis, M. Valente, C. Castiglioni, Dynamic response of composite frames with different shear connection degree, J. Construct. Steel Res. 65 (2009) 2050–2061.
[9] S. Di Benedetto, A. Francavilla, M. Latour, V. Piluso, G. Rizzano, Experimental response of a large-scale two-storey steel building equipped with low-yielding friction joints, Soil Dyn. Earthq. Eng. 152 (2021) http://dx.doi.org/10.1016/j.soildyn.2021.107022.
[10] V. Piluso, R. Montuori, E. Nastri, A. Paciello, Seismic response of MRF-CBF dual systems equipped with low damage friction connections, J. Construct. Steel Res. 135 (2019) 123–136.
[11] F. Freddi, C. Dimopoulos, T. Karavasilis, Experimental evaluation of a rocking damage-free steel column base with friction devices, J. Struct. Eng. 146 (2020) http://dx.doi.org/10.1061/(ASCE)ST.1943-541X.0002779.
[12] R.W.K. Chan, F. Albermani, Experimental study of steel slit damper for passive energy dissipation, Eng. Struct. 30 (2007) 1058–1066.
[13] S.-H. Oh, Y.-J. Kim, H.-S. Ryu, Seismic performance of steel structures with slit dampers, Eng. Struct. 31 (2009) 1997–2008.
[14] S.M.S. Alehashem, A. Keyhani, H. Pourmohammad, Behavior and performance of structures equipped with ADAS and TADAS dampers (a comparison with conventional structures), in: 14th World Conference on Earthquake Engineering, Beijing, China, 2008.
[15] J. Lanning, C.-M. Uang, Testing and modeling of a36 and stainless steel buckling-restrained braces under near-fault loading conditions, in: 5th Asia Conference on Earthquake Engineering, Taipei, Taiwan, 2014.
[16] L. Di Sarno, A.S. Elnashai, D.A. Nethercot, Seismic retrofitting of framed structures with stainless steel, J. Construct. Steel Res. 62 (2006) 93–104.
[17] J.C. De la Llera, C. Esguerra, J.L. Almazàn, Earthquake behaviour of structures with copper energy, Earthq. Eng. Struct. Dyn. 33 (2004) 329–358.
[18] M. D'Aniello, G. La Manna Ambrosino, F. Portioli, R. Landolfo, Role of compression diagonals in concentrically braced frames in moderate seismicity: A full scale experimental study, Steel Compos. Struct. 15 (5) (2013) 539–566.
[19] P. Uriz, F.C. Filippou, S.A. Mahin, Model for cyclic inelastic buckling of steel braces, J. Struct. Eng. 134 (4) (2008) 619–628.
[20] A. Kanyilmaz, Role of compression diagonals in concentrically braced frames in moderate seismicity: A full scale experimental study, J. Construct. Steel Res. 133 (2017) 1–18.

[21] F. Freddi, E. Tubaldi, A. Zona, A. Dall'Asta, Seismic performance of dual systems coupling momentresisting and buckling-restrained braced frames, Earthq. Eng. Struct. Dyn. (2020) http://dx.doi.org/10.1002/eqe.3332.
[22] A. Zona, L. Ragni, A. Dall'Asta, Sensitivity-based study of the influence of brace over-strength distributions on the seismic response of steel frames with BRBs, Eng. Struct. 37 (2012) 179–192.
[23] C. Black, N. Makris, I. Aiken, Component testing, seismic evaluation and characterization of BRBs, J. Struct. Eng. 130 (2002) 880–894.
[24] I. Vayas, Innovative Anti-Seismic Devices and Systems, ECCS - European Convention for Constructional Steework, Baffins Lane, Chichester West Sussex PO19 1ud, England, ISBN: 978-92-9147- 136-2, 2017.
[25] A. Plumier, et al., Two Innovations for Earthquake-Resistant Design: the INERD Project, INERD Final Report, Contract number 7210-PR-316, Research Fund for Coal and Steel, 2004.
[26] I. Vayas, P. Karydakis, D. Dimakogianni, G. Dougka, C.A. Castiglioni, A. Kanyilmaz, L. Calado, J.M. Proenca, M. Espinha, B. Hoffmeister, T. Rauert, D. Kalteziotis, Dissipative Devices for Seismic Resistant Steel Frames (Fuseis) - Final Report, Tech. Rep., National Technical University of Athens, Politecnico di Milano, Instituto Superior Técnico Lisboa, RWTH Aachen University, SIDENOR SA, 2011.
[27] M. Valente, C. Castiglioni, A. Kanyilmaz, Dissipative devices for earthquake resistant composite steel structures: bolted versus welded solution, Bull. Earthq. Eng. 14 (2016) 3613–3639.
[28] G. Abbiati, O.S. Bursi, P. Caperan, L. Di Sarno, F.J. Molina, F. Paolacci, P. P, Hybrid simulation of multi-span RC viaduct with plain bars and sliding bearings, Earthq. Eng. Struct. Dyn. 44 (2015) 2221–2240.
[29] O.S. Bursi, G. Abbiati, E. Cazzador, P. Pegon, F.J. Molina, F. Paolacci, P. Pegon, Nonlinear heterogeneous dynamic substructuring and partitioned FETI time integration for the development of low-discrepancy simulation models, Int. J. Numer. Methods Eng. 112 (2017) 1253–1291.
[30] G. Xu, Z. Wang, B. Wu, O.S. Bursi, X. Tan, Q. Yang, L. Wen, H. Jiang, Pseudodynamic tests with substructuring of a full-scale precast box-modularized structure made of reinforced concrete shear walls, Struct. Des. Tall Special Build. 26 (2017).
[31] A.M. Reinhorn, M. Bruneau, S.Y. Chu, X. Shao, P.M. C., Large scale real time dynamic hybrid testing technique - shake tables substructure testing, in: 2003 Structures Congress and Exposition, Seattle, 2003.
[32] M.J. Hashemi, G. Mosqueda, Innovative substructuring technique for hybrid simulation of multistory buildings through collapse, Earthq. Eng. Struct. Dyn. 43 (2014) 2059–2074.
[33] A. Kanyilmaz, C.A. Castiglioni, et al., DISSIPABLE Proposal, Tech. Rep., Politecnico di Milano, Instituto Superior Técnico Lisboa, University of Trento, RWTH Aachen University, National Technical University of Athens NTUA, RINA Consulting - Centro Sviluppo Materiali SpA, University of Pisa, SOFMAN, 2017.
[34] F. Mattei, G. Giuliani, R. Andreotti, S. Caprili, N. Tondini, Experimental and numerical assesment of a steel frame equipped with dissipative replaceable bracing connections, Proc. Struct. Integr. 44 (2023) 1204–1211.
[35] I. Vayas, P. Thanopoulos, Innovative dissipative (INERD) pin connections for seismic resistant braced frames, Steel Struct. 5 (2005).
[36] Computers, S. Inc., SAP2000 integrated software for structural analysis and design, 2023, https://www.csiamerica.com/products/sap2000.
[37] CEN, EN 1993-1-1 - Eurocode 3: Design of Steel Structures - Part 1-1: General Rules and Rules for Buildings, CEN - European Committee of Standardization, Bruxelles, 2005.
[38] CEN, EN 1993-1-8 - Eurocode 3: Design of Steel Structures - Part 1-8: Design of Joints, CEN - European Committee of Standardization, Bruxelles, 2005.
[39] CEN, EN 1994-1 - Eurocode 4: Design of Composite Steel and Concrete Structures - Part 1.1: General Rules, and Rules for Buildings, CEN - European Committee of Standardization, Bruxelles, 2004.
[40] F. McKenna, G.L. Fenves, M. Scott, OpenSees: Open System for Earthquake Engineering Simulation, University of California Berkeley, 2006, opensees.berkeley.edu.
[41] A. Kanyilmaz, C.A. Castiglioni, et al., Fully Dissipative and Easily Repairable Components for Resilient Buildings with Composite Steel-Concrete Structures, DISSIPABLE Final Report, Grant Agreement No 800699, Research Fund for Coal and Steel, 2022.
[42] L. Calado, J.M. Proenca, M. Espinha, C.A. Castiglioni, Hysteretic behaviour of dissipative bolted fuses for earthquake resistant steel frames, J. Construct. Steel Res. 85 (2013) 151–162.
[43] C. Chisari, A. Francavilla, M. Latour, V. Piluso, G. Rizzano, C. Amadio, Critical issues in parameter calibration of cyclic models for steel members, Eng. Struct. 132 (2017) 123–138.
[44] G. Giuliani, R. Andreotti, N. Tondini, O.S. Bursi, Experimental analysis of steel frames protected with easily repairable dissipative seismic devices, in: XI International Conference on Structural Dynamics, Athens, Greece, 2020.
[45] CEN, EN 1998-1 - Eurocode 8: Design of Structures for Earthquake Resistance - Part 1: General Rules, Seismic Actions and Rules for Buildings, Working draft, CEN - European Committee of Standardization, Bruxelles, 2018.
[46] C. Farhat, F.-X. Roux, A method of finite element tearing and interconnecting and its parallel solution algorithm, Numer. Methods Eng. 32 (6) (1991) 1205–1227.
[47] G. Abbiati, I. Lanese, E. Cazzador, O.S. Bursi, A. Pavese, A computational framework for fast-time hybrid simulation based on partitioned time integration and state-space modeling, Struct. Control Health Monit. 26 (e2419) (2019).
[48] R.R. Craig, A. Kurdila, Fundamentals of Structural Dynamics, JOHN WILEY and SONS, INC, 2006.
[49] G. Abbiati, P. Covi, N. Tondini, O. Bursi, B. Stojadinovic, A real-time hybrid fire simulation method based on dynamic relaxation and partitioned time integration, J. Eng. Mech. 146 (9) (2020) http://dx.doi.org/10.1061/(ASCE)EM.1943-7889.0001826.
[50] ECCS, Recommended Testing Procedure for Assessing the Behaviour of Structural Steel Elements under Cyclic Loads, ECCS Publication n.45, ECCS, Bruxelles, 1986.